

# Oxygen Isotope ( $^{18}\text{O}_2$ ) Evidence on the Role of Oxygen in the Plasma-Driven Catalysis of VOC Oxidation

Hyun-Ha Kim · Atsushi Ogata · Milko Schiorlin ·  
Ester Marotta · Christina Paradisi

Received: 8 August 2010 / Accepted: 29 October 2010 / Published online: 16 November 2010  
© Springer Science+Business Media, LLC 2010

**Abstract** This paper reports isotopic evidence on non-thermal plasma-induced fixation of gas-phase oxygen on the surface of several catalysts such as  $\text{TiO}_2$ ,  $\text{Ag}/\text{TiO}_2$ ,  $\text{Ag}/\gamma\text{-Al}_2\text{O}_3$  and  $\text{Ag}/\text{MS}-13\text{X}$  at atmospheric-pressure. On-line mass spectrometric analysis and stoichiometric comparison of reactants and products revealed that the fixed surface oxygen can be activated by nonthermal plasma. The fixed  $^{18}\text{O}$  by nonthermal plasma survived for a certain period of time (about 30 min), and involved in the formation of isotope-exchanged oxygen ( $^{18}\text{O}^{16}\text{O}$ ) and isotope containing  $\text{CO}_x$  ( $\text{CO}$  and  $\text{CO}_2$ ).

**Keywords** Plasma-driven catalysis · Heterogeneous catalyst · Isotope oxygen · VOC oxidation

## 1 Introduction

Atmospheric-pressure nonthermal plasma (NTP) offers unique chemical environment for the removal of dilute air pollutants. Electrical energy is converted into chemically reactive species in the plasma. On the other hand, extensive studies during the last two decades pointed out several limitations of the plasma alone processes for the extended practical use in industry. These include large energy consumption, low selectivity, and formation of unwanted byproducts. Combination of nonthermal plasma with

heterogeneous catalyst is currently considered as a possible way to overcome these problems. Two types of combination, single-stage and two-stage, are currently being studied to improve the process performance. Single-stage process is more complex compared to two-stage process, and little knowledge is presently available on the interaction between plasma and catalyst. Nevertheless, this complementary combination has been experimentally proved to provide better selectivity for plasma and lower working temperature for catalyst [1–3]. For example, it has been reported that the combination of dielectric barrier discharge plasma and manganese catalyst enhances TCE decomposition and  $\text{CO}_2$  selectivity [4, 5]. The loading of active metals not only enhance  $\text{CO}_2$  selectivity for various VOCs [6–8], but also extend plasma area over the surface of catalyst [9]. The important role of oxygen was confirmed by varying  $\text{O}_2$  content in gas mixtures. The larger the oxygen content, the higher the decomposition efficiency of VOC and the  $\text{CO}_2$  selectivity [10, 11].

Fundamental research works are under progress for a better understanding of the interaction between plasma and catalyst. Roland et al. experimentally studied the stabilization of plasma-formed oxidants on the surface of  $\text{LaCoO}_3$  [12]. When  $\text{CO}/\text{N}_2$  mixture was fed to the plasma pretreated  $\text{LaCoO}_3$  catalyst, the profiles of outlet CO concentration exhibited different patterns according to the plasma pretreatment time. As the plasma treatment time increased, the recovery of outlet CO concentration became slower. Although the profile of  $\text{CO}_2$  was not given, the authors tentatively explained the difference of CO profile due to the oxidation induced by surface atomic oxygen fixed by the plasma. Holzer et al. also studied the interaction between nonthermal plasma and catalysts for both single-stage and two-stage configuration [13]. They also consider the role of porosity and the possible adsorption of

H.-H. Kim (✉) · A. Ogata  
National Institute of Advanced Industrial Science  
and Technology (AIST), Tsukuba 305-8569, Japan  
e-mail: hyun-ha.kim@aist.go.jp

M. Schiorlin · E. Marotta · C. Paradisi  
Department of Chemical Science, Padova University,  
Padova, Italy

atomic oxygen (or ozone) on the surface of the catalyst. More recently, Guaitella et al. have shown that the plasma pretreated  $\text{TiO}_2$  with  $\text{O}_2$  or air can remove  $\text{C}_2\text{H}_2$  even in the absence of plasma and UV activation [14]. The adsorbed oxygen species were considered to play a key role in those experiments.

Experiments with stable isotopes and mass spectrometric analysis provide a powerful tool to study the mechanism of chemical reactions. Isotopically-labeled chemicals have been used in the gas-phase chemistry of nonthermal plasma and electron-beam irradiation. Locke et al. studied the nonthermal plasma decomposition of  $\text{NOx}$  in  $^{15}\text{NO-N}_2$  mixture [15]. Martin et al. studied the decomposition mechanism of toluene in a point-plane type barrier discharge using  $^{18}\text{O}_2$  and deuterium-labeled toluene ( $\text{C}_6\text{H}_6\text{-CD}_3$ ) [16]. Material balance of nitrogen oxides in electron-beam processing of simulated flue gas was studied using  $^{15}\text{N}$  labeled NO [17, 18]. Oxygen isotope ( $^{18}\text{O}_2$ ) has been used in many catalytic reactions to understand the mechanism involving oxygen. Calla and Davis used  $^{18}\text{O}_2$  to study the CO oxidation over titania- and alumina-supported Au nanoparticles [19]. The behavior of oxygen under discharge plasma over catalyst has been investigated using  $^{18}\text{O}_2$  at atmospheric pressure and room temperature. Measured data of reaction products provides a direct evidence for the plasma induced fixation of oxygen on the catalyst surface and its subsequent involvement in the oxidation of VOC.

In this work, we measured the profile of isotope oxygen species in plasma-driven catalyst reactor packed with four catalysts,  $\text{TiO}_2$ ,  $\text{Ag/TiO}_2$ ,  $\text{Ag}/\gamma\text{-Al}_2\text{O}_3$  and  $\text{Ag/MS-13X}$ . The chemical change by the plasma was evaluated based on the stoichiometric ratio between reactants and products.

## 2 Experimental

Figure 1 shows the experimental setup used in this study. A barrier type plasma reactor packed with catalysts was used.

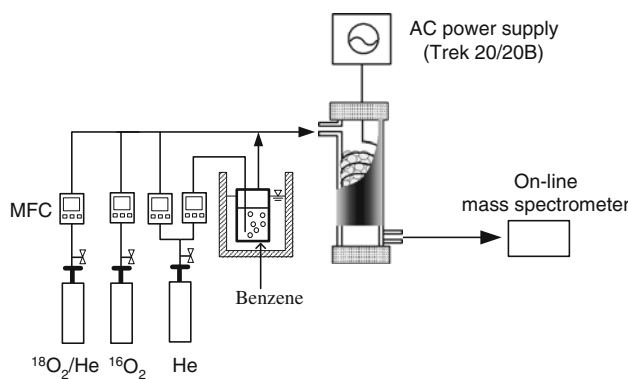


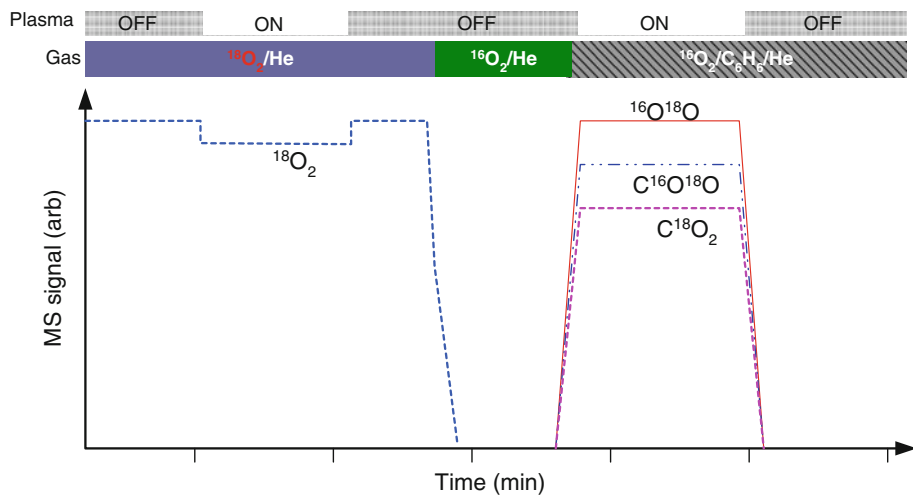
**Fig. 1** Experimental setup

The effective length and inner diameter were 40 and 8 mm, respectively. The coil electrode (stainless steel with 0.45 mm diameter) was set at the inner surface of the quartz tube, which served as a corona electrode. Silver paste was painted on the outer surface as a ground electrode. Three different catalysts either in pellet or bead were tested. Gamma alumina (Mizusawa Chemical Co.) and anatase type of  $\text{TiO}_2$  (Sakai Chemicals Co.) were spherical beads with average diameter of about 1.8 and 2.0 mm, respectively. Molecular sieve-13X (MS-13X, Sigma-Aldrich Co.) was pellet with 1.6 mm diameter and 2 mm length. The MS-13X has the specific surface area of  $540 \text{ m}^2 \text{ g}^{-1}$ , and followed by  $\gamma\text{-Al}_2\text{O}_3$  ( $210 \text{ m}^2 \text{ g}^{-1}$ ) and  $\text{TiO}_2$  ( $60 \text{ m}^2 \text{ g}^{-1}$ ). Silver was impregnated on the surface of catalyst using  $\text{AgNO}_3$  as a precursor. The resulting catalysts were dried using a rotary evaporator, and then calcined at  $500^\circ\text{C}$  in air for 10 h.

The plasma-catalyst reactor was energized by an AC power supply (Trek, Model 20/20B). Frequency and applied voltage were fixed at 200 Hz and  $24 \text{ kV}_{\text{pk-pk}}$ , respectively. Applied voltage was measured by a high voltage probe (Tektronix, P6015A) and an oscilloscope (Tektronix, TDS3034B). Discharge power was measured by using a V-Q Lissajous figure program (Insight Co. Version 1.72) [20]. The typical discharge power in the catalyst-packed plasma reactor was in the range of 2.1–2.4 W.

The gas components were measured by an on-line mass spectrometer (MKS Residual Gas Analyzer Microvision-IP) equipped with a quadrupole mass analyzer and a Faraday cup or a multiplier as detector (MKS Instruments). In the present experiments the multiplier was used preferentially as it offered higher sensitivity. The mass range was set from  $m/z$  4 to 80 according to the gas mixtures of reactants and products. The isotope-labelled oxygen ( $^{18}\text{O}_2$ ) with purity of 99.9% was supplied from Cambridge Isotope Laboratories, Inc and it was diluted with high purity He (99.999% purity, Takachiho Co.). The purity of normal oxygen ( $^{16}\text{O}_2$ ) was 99.999%. For the convenience of experiment, oxygen concentration was set at 2.5% for  $^{18}\text{O}_2/\text{He}$  or  $^{16}\text{O}_2/\text{He}$ . The  $^{16}\text{O}^{18}\text{O}$  can be formed in the ionizer of the mass spectrometer when  $^{16}\text{O}_2$  and  $^{18}\text{O}_2$  were coexisted in sample gas mixture. The intensity of  $^{16}\text{O}^{18}\text{O}$  was found to be about 3–5% of the inlet oxygen molecules ( $^{16}\text{O}_2 + ^{18}\text{O}_2$ ). In the experimental conditions of this study,  $^{18}\text{O}_2$  and  $^{16}\text{O}_2$  did not coexist so the formation of  $^{16}\text{O}^{18}\text{O}$  in the mass spectrometer ionizer can be neglected. Benzene was supplied by bubbling liquid benzene with  $10 \text{ mL min}^{-1}$  He flow. The gas flow rate was regulated using mass flow controllers (KOFLOC, FCC-3000). Reaction temperature was in the range of 293–300 K at atmospheric pressure. Total gas flow rate was  $0.2 \text{ L min}^{-1}$  at standard conditions (273 K, 0.1 MPa). All experiments

**Fig. 2** Experimental procedure flow-chart



were conducted at dry conditions. Humidity was less than about 80 ppmv, as measured by a dew point hygrometer (General Eastern, Hygro-M4 Model).

Figure 2 shows the experimental scheme for the isotope exchange experiment. In the first step, 2.5%  $^{18}\text{O}_2$  in He was fed to the reactor and, after a few minutes, the discharge plasma was turned on. After 10 min the plasma was turned off, the gas flow was switched from  $^{18}\text{O}_2/\text{He}$  to  $^{16}\text{O}_2/\text{He}$  and kept for about 30 min. The benzene flow was then started and after about 3 min the plasma was turned on again. In this second step of plasma application, oxidation products of benzene, especially those containing  $^{18}\text{O}$ , were measured together with the isotope-exchange product,  $^{18}\text{O}^{16}\text{O}$ .

Table 1 summarizes mass number of oxygen-containing species, which could be detected in this study. In the case of nitrogen dilution, some of mass number overlaps with isotope-exchanged species. For example,  $\text{C}^{18}\text{O}$  and  $\text{N}^{16}\text{O}$  have the same mass number ( $m/z$  30). To identify the mass signals of oxygen species more correctly, helium was used instead of  $\text{N}_2$  as dilution gas.

### 3 Results and Discussions

Figure 3 shows the profiles of oxygen species in the plasma reactors packed with four different catalysts. The catalytic activity in VOC decomposition and the some physical-, electrical properties of these catalysts have been reported elsewhere [9, 11, 20]. The signal of normal oxygen,  $^{16}\text{O}_2$ , was observed as an impurity in the  $^{18}\text{O}_2/\text{He}$  flow. Since the MS signal intensity was linearly proportional to oxygen concentration up to about 3% within reasonable error limits, the impurity level of  $^{16}\text{O}_2$  was estimated to be about 400–500 ppm. Interestingly, some isotope-exchanged oxygen  $^{16}\text{O}^{18}\text{O}$  was observed as the  $^{18}\text{O}_2$  feeding started

**Table 1** Mass to charge ratios ( $m/z$ ) for the isotope exchange reactions

$m/z$	With He dilution	With $\text{N}_2$ dilution
16	$^{16}\text{O}$	
18	$^{18}\text{O}$	
28	$\text{C}^{16}\text{O}$	$\text{N}_2$
30	$\text{C}^{18}\text{O}$	$\text{N}^{16}\text{O}$
32	$^{16}\text{O}_2$	$\text{N}^{18}\text{O}$
34	$^{16}\text{O}^{18}\text{O}$	
36	$^{18}\text{O}_2$	
44	$\text{C}^{16}\text{O}_2$	$\text{N}_2^{16}\text{O}$
46	$\text{C}^{16}\text{O}^{18}\text{O}$	$\text{N}^{16}\text{O}_2$
48	$\text{C}^{18}\text{O}_2, ^{16}\text{O}_3$	$\text{N}^{16}\text{O}^{18}\text{O}$
50	$^{16}\text{O}_2^{18}\text{O}$	$\text{N}^{18}\text{O}^{18}\text{O}$
52	$^{16}\text{O}^{18}\text{O}_2$	
54	$^{18}\text{O}_3$	

even in the absence of plasma application. The intensity of  $^{16}\text{O}^{18}\text{O}$  was larger than that of the impurity  $^{16}\text{O}_2$ . This result indicates that the heterogeneous catalytic reaction is the main reason for the  $^{16}\text{O}^{18}\text{O}$  signal without plasma ON. Application of plasma caused a sharp increase of the  $^{16}\text{O}^{18}\text{O}$  signal, which was estimated to reach a concentration around 2000–2500 ppm. Electrical discharge is known as an effective way to achieve the gas-phase isotope exchange equilibrium [21]. It should be noted that formation of  $^{16}\text{O}^{18}\text{O}$  requires the consumption of equal amounts of  $^{16}\text{O}_2$  and  $^{18}\text{O}_2$ . If we assume that the impurity  $^{16}\text{O}_2$  is the only source of  $^{16}\text{O}$  and that  $^{16}\text{O}^{18}\text{O}$  can only form by the gas-phase Reaction R1, then the ratio of  $^{16}\text{O}^{18}\text{O}$  formation to  $^{18}\text{O}_2$  consumption should be no larger than two.



However, the ratio of  $^{16}\text{O}^{18}\text{O}$  to the initial  $^{16}\text{O}_2$  ranged from 3.3 to 4.6 indicating that considerable amounts of  $^{16}\text{O}$

were supplied by sources other than gas-phase  $^{16}\text{O}_2$ . Catalyst surface is expected to be a probable source of  $^{16}\text{O}$ , because oxygen is fixed on the surface in various forms. The presence of surface oxygen radical anions ( $\text{O}^-$ ,  $\text{O}^{2-}$ ,  $\text{O}_2^-$ ), metal oxide and lattice oxygen have been measured by various techniques such as ESR (electron spin resonance), temperature-programmed desorption (TPD), x-ray photoelectron spectroscopy (XPS) etc. [22, 23]. The involvement of surface oxygen can be further validated by the ratio of the  $^{16}\text{O}^{18}\text{O}$  increase to the  $^{16}\text{O}_2$  decrease by a plasma application. These values were in the range of 2.8–7.5, indicating more  $^{16}\text{O}^{18}\text{O}$  formation than the consumption of impurity  $^{16}\text{O}_2$  in the gas-phase. Mass spectrometric measurements of isotope oxygen species provided clear evidence that the atmospheric-pressure plasma can activate surface oxygen species fixed on catalysts. On the other hand, the signal of  $^{18}\text{O}_2$  slightly decreased in the presence of discharge plasma. This value went back to its initial value after the plasma was turned off. These trends are common to all tested catalysts. The contribution of silver (Ag) can be seen from the comparison between (a)  $\text{TiO}_2$  and (b) 4% Ag/ $\text{TiO}_2$ . The produced amount of  $^{16}\text{O}^{18}\text{O}$  was larger with 4% Ag/ $\text{TiO}_2$  than with  $\text{TiO}_2$  alone. The signal of ozone was not detected.

The gas flow was then switched from  $^{18}\text{O}_2/\text{He}$  to  $^{16}\text{O}_2/\text{He}$  and kept for about 30 min, and then eventually set to  $\text{C}_6\text{H}_6/\text{He}$ . Figure 4 shows the time-lapse changes for the intensity of relevant ion signals observed in the presence of different catalysts. It should be noticed that the outlet benzene concentration was always below the detection limits because the adsorption equilibrium requires much longer time than the measurement time-scale. The profiles of benzene decomposition products (CO and  $\text{CO}_2$ ) are also not in steady state. Because of the high purity of  $^{16}\text{O}_2$ , the  $^{18}\text{O}_2$  signal was kept to decrease with time after switching the gas line. Nevertheless, as already indicated in Fig. 3, a constant  $^{16}\text{O}^{18}\text{O}$  signal was observed even in the absence of plasma. This observation provides even more convincing evidence of the heterogeneous pathway for the  $^{16}\text{O}^{18}\text{O}$  formation. When the plasma was turned on again with benzene/ $^{16}\text{O}_2/\text{He}$  flow, several reaction products containing  $^{18}\text{O}$  were observed. The most abundant one was  $^{16}\text{O}^{18}\text{O}$ . Despite the same reaction conditions, the increase of  $^{16}\text{O}^{18}\text{O}$  by the plasma was more significant than that observed with all catalysts in the absence of benzene (Fig. 3). One possible reason for this discrepancy is the isotope effect in the reaction rate. Reaction rate coefficients of isotopically-labeled oxygen ( $^{18}\text{O}_2$ ) differ from normal

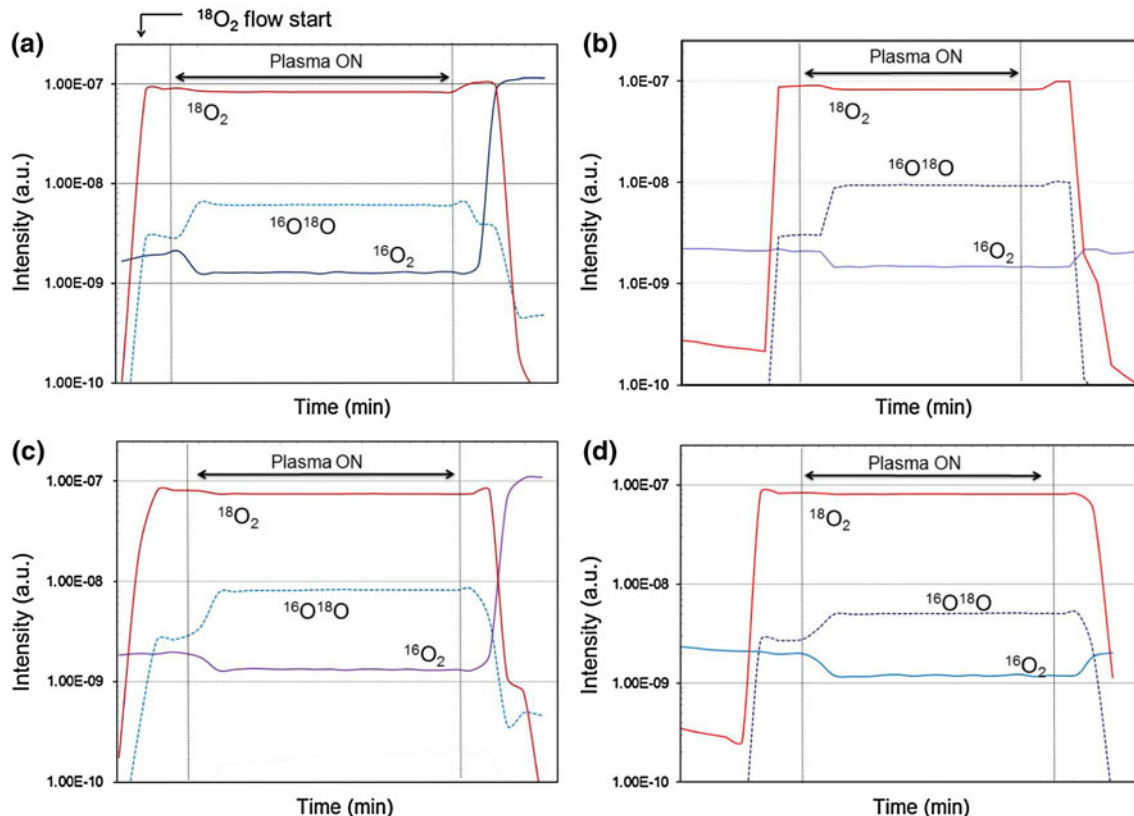


**Fig. 3** Evolution of reaction products from  $^{18}\text{O}_2/\text{He}$  mixture; **a**  $\text{TiO}_2$  catalyst, **b** 4% Ag/ $\text{TiO}_2$  catalyst, **c** 5% Ag/ $\gamma\text{-Al}_2\text{O}_3$  catalyst, and **d** 5% Ag/MS-13X catalyst. Plasma was applied for 10 min

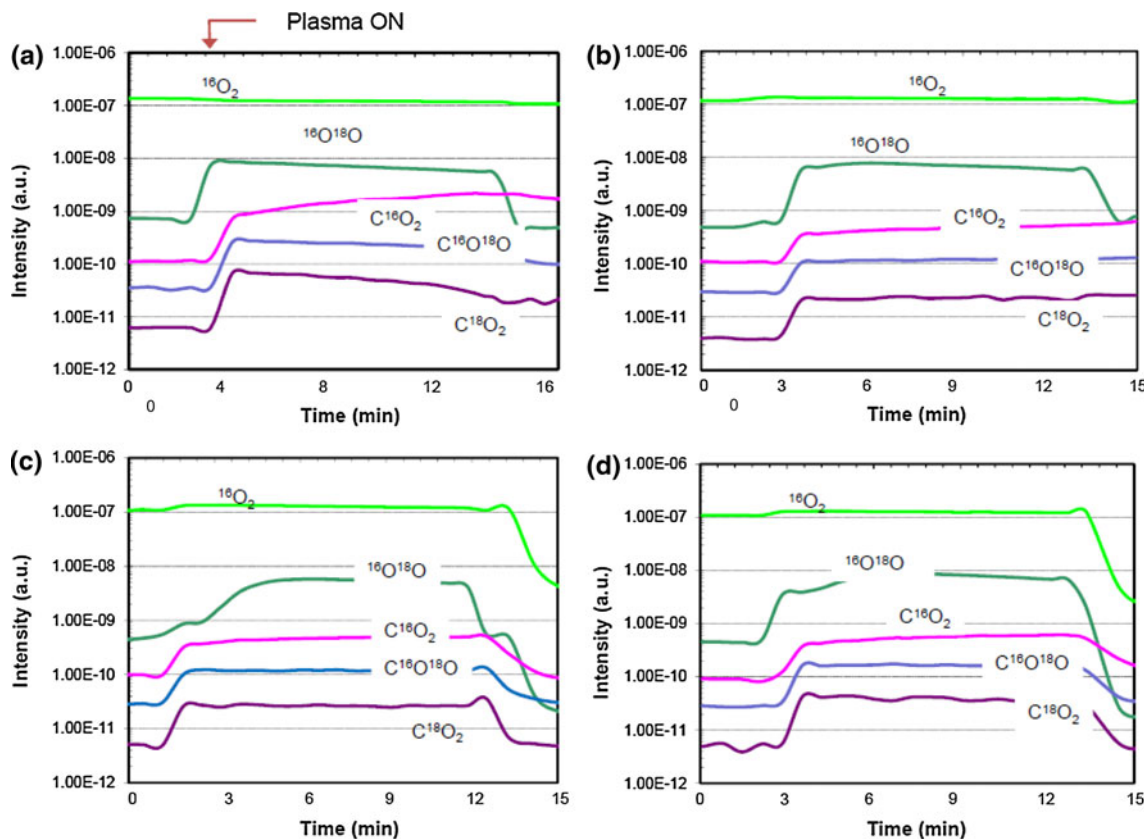
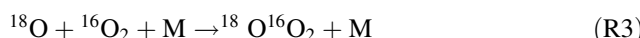


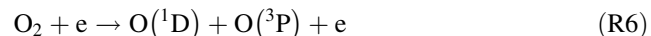
**Fig. 4** Evolution of reaction products from  $^{16}\text{O}_2/\text{He}$  mixture containing benzene; **a**  $\text{TiO}_2$  catalyst, **b** 4%  $\text{Ag}/\text{TiO}_2$  catalyst, **c** 5%  $\text{Ag}/\gamma\text{-Al}_2\text{O}_3$  catalyst, and **d** 5%  $\text{Ag}/\text{MS-13X}$  catalyst. Catalysts were pretreated in  $^{18}\text{O}_2/\text{He}$  mixture for 10 min (see Fig. 3)

oxygen ( $^{16}\text{O}_2$ ). Two well-known examples are the ozone formation [24, 25] and isotope-exchange reaction [26, 27]. Thus, the reaction rate coefficient of  $k_{R2}$  is known to be 50% larger than  $k_{R3}$  [28, 29].



Similarly, the reaction rate coefficient  $k_{R5}$  is 1.25 times larger than  $k_{R4}$ . If we assume that surface  $^{18}\text{O}_s$  reacts more easily than surface  $^{16}\text{O}_s$ , then the observed data can be well explained. It is interesting to note that the  $^{18}\text{O}$  containing products decreased with time in the case of  $\text{TiO}_2$ , whereas the  $\text{C}^{16}\text{O}_2$  kept increasing. On the other hand, Ag loaded catalysts exhibited constant levels of  $^{18}\text{O}$  containing products. These observations suggest that the Ag nanoparticles play an important role as oxygen ( $^{18}\text{O}_2$  in this case) reservoirs. It has been well-known that active metals are capable of adsorbing oxygen on their surface. Oxygen adsorption on silver has also been the object of intensive study because of its peculiar activity toward ethylene partial oxidation to ethylene oxide [30, 31]. For

example, Busser et al. studied the temperature-programmed desorption (TPD) of  $\text{O}_2$  from  $\text{Ag}/\text{Al}_2\text{O}_3$  catalyst in a microreactor [32]. Bukhtiyarov et al. reported that the size of silver particles substantially changed the oxygen adsorption pattern [31, 33]. Recently, enhanced interaction of plasma with silver nanoparticle loaded zeolites has been demonstrated by the microscope-ICCD camera measurement [9]. Regardless of the type of surface oxygen species, it is evident that the  $^{18}\text{O}$  was supplied from the surface of catalysts, which was fixed by discharge plasma in  $^{18}\text{O}_2/\text{He}$  flow. The most prominent decomposition product of benzene was  $\text{C}^{16}\text{O}_2$  and followed by  $\text{C}^{16}\text{O}^{18}\text{O}$  and  $\text{C}^{18}\text{O}_2$ . This order was the same for all tested catalysts in this study. In the case of benzene/ $^{16}\text{O}_2/\text{He}$  mixture, the signal changes of  $^{16}\text{O}_2$  were less significant compared to those of  $^{18}\text{O}_2/\text{He}$  mixture. Although the detailed reason for this is not clear at this stage, unknown behavior of oxygen isotope could be a reason. Weston pointed out that significant kinetic isotope effects are found in the electron impact dissociation of molecular oxygen, R6 [34].



Thus, the reaction rates for the electron impact dissociation of  $^{17}\text{O}^{16}\text{O}$  and  $^{18}\text{O}^{16}\text{O}$  are two times faster

than that of  $^{16}\text{O}_2$ . Within our literature survey, there is no previous report on the reaction rate of R6 for  $^{18}\text{O}_2$ . If  $^{18}\text{O}_2$  dissociates more easily than  $^{16}\text{O}_2$ , similarly to  $^{17}\text{O}^{16}\text{O}$  and  $^{18}\text{O}^{16}\text{O}$ , then the different profile of oxygen ( $^{18}\text{O}_2$  and  $^{16}\text{O}_2$ ) in  $^{18}\text{O}_2/\text{He}$  and  $^{16}\text{O}_2/\text{He}$  can be rationalized. In conclusion, although, the nature of the kinetically active oxygen species in these systems is still uncertain, it was found that nonthermal plasma can induce fixation of oxygen on the surface of catalyst and chemical reaction as well. Remaining open questions are what are the surface oxygen species fixed by a discharge plasma and how do they interact with discharge plasma which leads to catalytic reaction on the surface. These will be further investigated in future studies.

#### 4 Summary

The role of oxygen in plasma-driven catalysis has been investigated using isotopically-labeled molecular oxygen ( $^{18}\text{O}_2$ ). It was found that oxygen is fixed onto the surface of the catalyst by the action of atmospheric-pressure non-thermal discharge plasma, and can survive in such a state for about 30 min. In turn, the adsorbed  $^{18}\text{O}$ -labeled oxygen species are easily activated by discharge plasma, and react with  $^{16}\text{O}_2$  and benzene to produce  $^{18}\text{O}^{16}\text{O}$  and  $^{18}\text{O}$ -containing  $\text{CO}_x$ , respectively. The Ag nanoparticles supported on catalysts served as oxygen reservoirs.

#### 5 Acknowledgment

This research was partly supported by the Environmental Research and Technology Development Fund (S2-01) of the Ministry of the Environment, Japan.

#### References

1. Kim HH (2004) Plasma Process Polym 1:91
2. Chen HL, Lee HM, Chen SH, Chang MB, Yu SJ, Li SN (2009) Environ Sci Technol 43:2216
3. Sano T, Negishi N, Sakai E, Matsuzawa S (2006) J Mol Catal A Chem 245:235
4. Magureanu M, Mandache NB, Parvulescu VI, Subrahmanyam C, Renken A, Kiwi-Minsker L (2007) Appl Catal B Environ 74:270
5. Han S-B, Oda T, Ono R (2005) IEEE Trans Ind Appl 41:1343
6. Kim HH, Oh SM, Ogata A, Futamura S (2004) Catal Lett 96:189
7. Hakoda T, Matsumoto K, Mizuno A, Kojima T, Hirota K (2008) Plasma Chem Plasma Proc 28:25
8. Rousseau A, Meshchanov AV, Roepcke J (2006) Appl Phys Lett 88:021503
9. Kim HH, Kim JH, Ogata A (2009) J Phys D Appl Phys 42:135210
10. Kim HH, Oh SM, Ogata A, Futamura S (2005) J Adv Oxid Technol 8:226
11. Kim HH, Ogata A, Futamura S (2008) Appl Catal B Environ 79:356
12. Roland U, Holzer F, Kopinke F-D (2002) Catal Today 73:315
13. Holzer F, Roland U, Kopinke F-D (2002) Appl Catal B Environ 38:163
14. Guaitella O, Lazzaroni C, Marinov D, Rousseau A (2010) Appl Phys Lett 97:011502
15. Locke BR, Clark RJ, Sathiamoorthy G, Finney WC (1997) NEDO symposium on non-thermal discharge plasma technology for air pollution control. Beppu, Japan, p 169
16. Martin L, Ognier S, Daou F, Amouroux J (2005) High Temp Mater Proc 9:531
17. Namba H, Tokunaga O, Suzuki R, Aoki S (1990) Appl Radiat Isot 41:569
18. Namba H, Aoki Y, Tokunaga O, Suzuki R, Aoki S (1988) Chem Lett 1465
19. Calla JT, Davis RJ (2006) J Catal 241:407
20. Kim HH, Ogata A, Futamura S (2006) IEEE Trans Plasma Sci 34:984
21. Ogg Jr RA, Sutphen WT (1953) J Chem Phys 21:2078
22. Panov GI, Dubkov KA, Starokon EV (2006) Catal Today 117:148
23. Bukhtiyarov VI, Kaichev VV, Prosvirin IP (1999) J Chem Phys 111:2169
24. Vetroshkin E, Babikova D (2007) J Chem Phys 127:154312
25. Anderson SM, Hulsebusch D, Mauersberger K (1997) J Chem Phys 107:5385
26. Fleurat-Lessard P, Grebenchikov SY, Schinke R, Janssen C, Krankowsky D (2003) J Chem Phys 119:4700
27. Chajia M, Jacon M (1994) J Chem Phys 101:271
28. Brenninkmeijer CAM, Janssen C, Kaiser J, Rockmann T, Rhee TS, Assonov SS (2003) Chem Rev 103:5125
29. Guenther J, Krankowsky D, Mauersberger K (2000) Chem Phys Lett 324:31
30. Kuroda Y, Mori T, Sugiyama H, Uozumi Y, Ikeda K, Itadani A, Nagao M (2009) J Colloid Interface Sci 333:294
31. Bukhtiyarov VI, Kaichev VV (2000) J Mol Catal A Chem 158:167
32. Busser GW, Hinrichsen O, Muhler M (2002) Catal Lett 79:49
33. Bukhtiyarov VI, Carley AF, Dollard LA, Roberts MW (1997) Surf Sci 381:L605
34. Weston Jr RW (1999) Chem Rev 99:2115